Efficient Orthonormal Function-based MPC for PMSM Drives in Domestic Appliances

Eleonora Brasili [1], Luigi Fagnano [2], Gianluca Ippoliti [3], Giuseppe Orlando [4]

Abstract—**This paper proposes a Model Predictive Control (MPC) strategy for the current regulation of Permanent Magnet Synchronous Motors (PMSMs) using Laguerre network expansions. While conventional MPC designs rely on forward shift operators to predict outputs, they often suffer from high computational complexity under rapid sampling or complex dynamics. By adopting a Laguerre-based functional expansion, the proposed method reduces the number of optimization parameters required for real-time implementation. Comparative analysis against industry-standard cascaded PI control—typical in high-volume domestic appliances—demonstrates that the Laguerre-MPC approach achieves superior dynamic performance with reduced computational overhead.**

Index Terms—**Model predictive control, permanent magnet synchronous motor, household appliance, Laguerre functions.**

I. Introduction

Driven by the availability of accurate plant models and the necessity for multi-constraint optimization, Model Predictive Control (MPC) has seen widespread adoption in power electronics and electrical drive systems [1]–[3].

MPC frameworks for power electronics are generally categorized into Continuous Control Set (CCS-MPC), which generates duty-cycle signals for a modulator [4], and Finite Control Set (FCS-MPC), which directly dictates the switching states of the power transistors [5]. While FCS-MPC reduces computational overhead and improves dynamic response relative to CCS-MPC [6], its variable switching frequency introduces significant component stress [7]. Furthermore, the inherent coupling between high switching frequency and controller sampling time, imposes the use of high-bandwidth digital controllers despite the simplicity of the underlying optimization algorithm. By decoupling controller sampling and switching intervals of power transistors, CCS-MPC ensures a fixed switching frequency [8]. Nevertheless, the computational complexity of solving the constrained optimization problem over an extended prediction horizon remains a primary bottleneck for implementation on resource-constrained hardware [9]. Comparative studies between FCS-MPC and CCS-MPC indicate that both strategies can achieve comparable steady-state and dynamic performance [10]. Nevertheless, CCS-MPC offers distinct advantages for industrial deployment: it maintains robustness at lower sampling rates, enables a fixed switching frequency, and decouples the modulation process from the control execution time. This decoupling is critical in industrial contexts to minimize switching losses and manage thermal stress. Furthermore, by utilizing a dedicated modulator, the switching frequency is no longer limited by the controller's sampling period, facilitating implementation on resource-constrained microcontroller units (MCUs).

This paper presents an online optimization-based CCS-MPC algorithm for current regulation in Permanent Magnet Synchronous Motors (PMSMs). The specific contribution is the integration of Laguerre-based parameterization within this framework, combining embedded integrator design, explicit voltage constraint handling, and simulation-based assessment, with the primary objective of generating optimal torque commands to track a prescribed speed trajectory under varying load conditions.

The use of the forward shift operator in CCS-MPC to parameterize the future control signal poses significant challenges for high-performance applications [11]. Specifically, rapid sampling rates and complex dynamics require a large number of parameters, which frequently results in excessive online computational demands. Drawing upon the framework established in [11], this study employs a parameterization of the control trajectory utilizing discrete orthogonal polynomial functions, i.e. a Laguerre network of suitable order. This parameterization facilitates a parsimonious and efficient representation of the future control signal, thereby reducing the total number of parameters required to model the control trajectory and allows the number of optimization variables to be reduced with respect to those necessitated by conventional shift-operator formulations.

The proposed control law was validated using a high-fidelity industrial simulation environment developed by Whirlpool for domestic appliance applications. Comparative analysis between the proposed MPC architecture and the industry-standard cascaded PI control currently deployed in production revealed substantial improvements in dynamic performance and regulation accuracy.

The paper is organized as follows: Section II introduces the PMSM state-space models, while Section III describes the vector control strategy. The MPC formulation using the Laguerre functions is outlined in Section IV, followed by numerical simulation in Section V. The paper concludes with Section VII.

[2]Luigi Fagnano is with *Whirlpool Technology Service S.r.l.* 60044 Fabriano (AN), Italy luigi_fagnano@whirlpool.com

[1]Eleonora Brasili, [3]Gianluca Ippoliti and [4]Giuseppe Orlando are with *Dipartimento di Ingegneria dell'Informazione* Università Politecnica delle Marche 60131 Ancona, Italy e.brasili@pm.univpm.it, gianluca.ippoliti@univpm.it, giuseppe.orlando@univpm.it.

II. MATHEMATICAL MODELING OF THE PMSM

The mathematical representation of the electrical subsystem of a isotropic PMSM, in the rotor-fixed (d, q) coordinate system, is expressed as follows:

$$\begin{cases} \dfrac{di_d(t)}{dt} = & -\dfrac{Ri_d(t)}{L} + \omega_e(t)i_q(t) + \dfrac{u_d(t)}{L} \\ \dfrac{di_q(t)}{dt} = & -\dfrac{Ri_q(t)}{L} - \omega_e(t)\left[i_d(t) + \dfrac{\lambda_0}{L}\right] + \dfrac{u_q(t)}{L} \end{cases} \quad (1)$$

In (1), the variables are defined as follows: $i_{d,q}$ and $u_{d,q}$ are the d-q frame stator currents and voltages; R and L are the stator resistance and inductance; λ_0 is the constant magnet flux linkage; and ω_e is the electrical rotor speed.

The electrical torque T_e is given by:

$$T_E(t) = K_t i_q(t). \quad (2)$$

The torque constant K_t is defined as $\frac{3}{2}\lambda_0 N_r$, where N_r is the pole pair count and ω_r is the mechanical rotor speed. As specified in [12], the absence of reluctance torque in this machine model results in a linear relationship between T_e and i_q.

The governing equations for the motor mechanics are as follows:

$$\begin{cases} \dfrac{d\theta_r(t)}{dt} = & \omega_r(t) \\ \dfrac{d\omega_r(t)}{dt} = & -\dfrac{B_f\omega_r(t)}{J_T} + \dfrac{T_E(t) - T_L(t)}{J_T} \end{cases} \quad (3)$$

where $\theta_r(t)$ and J_T are the rotor mechanical position and total inertia, respectively; B_f is the viscous friction coefficient; T_L is the unknown load torque.

The transformation between electrical and mechanical variables is established via the number of pole pairs, N_r:

$$\omega_e(t) = N_r\omega_r(t); \qquad \theta_e(t) = N_r\theta_r(t). \quad (4)$$

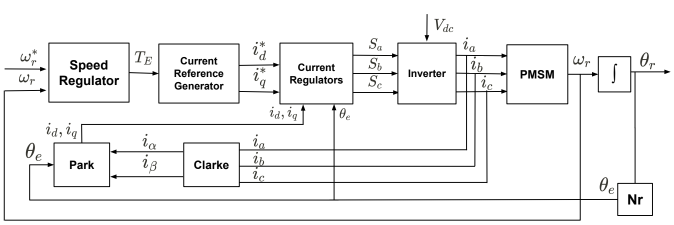

Fig. 1: FOC scheme for the PMSM

III. FIELD-ORIENTED MPC DESIGN

Field-Oriented Control (FOC) is a well-established methodology for regulating stator currents via vector control in the synchronous $d-q$ reference frame. The fundamental principle of FOC lies in a coordinate transformation that decouples the torque and flux dynamics, allowing for independent control of both quantities. This decoupling is performed within the rotating $d - q$ frame, as depicted in the control architecture shown in Fig. 1 [12].

The control hierarchy is structured into two cascaded loops:

- *Inner Current Loop:* Responsible for high-bandwidth regulation of the d- and q-axis currents. In standard operating regimes—excluding field-weakening regions—the direct-axis current reference i_d^* is maintained at zero to ensure constant flux linkage and maximize torque-per-ampere efficiency [12].
- *Outer Speed Loop:* Governs the mechanical angular velocity by generating the required electromagnetic torque command T_e^*.

Since the electromagnetic torque is governed by the quadrature-axis current i_q as defined in (2), the speed controller generates a target current i_q^* via the relationship $i_q^* = T_e^*/K_t$. The inner loop then regulates i_q to track this reference, ensuring the desired torque delivery. The regulation of stator currents and motor speed is achieved, in standard FOC architecture, using Proportional-Integral (PI) controllers.

Compared to standard PI-FOC, the proposed scheme replaces the outer-loop PI speed controller with a discrete-time Sliding Mode controller for speed regulation, and the inner-loop PI current controllers with an MPC-based strategy to enable a more rigorous handling of electrical constraints. Details of the Sliding Mode control implementation and analytical formulation are omitted for brevity and can be found in [13]. The integration of MPC in the inner loop allows for the explicit modeling of stator voltage limits as hard constraints within the optimization problem, enhancing transient response while guaranteeing equipment safety.

IV. COMPUTATIONALLY EFFICIENT MPC DESIGN USING LAGUERRE FUNCTIONS

The MPC formulation is derived by linearizing the current dynamics (1) around a nominal speed ω_n. Utilizing the forward Euler approximation with sampling interval Δt, the system is transformed into the following discrete-time linear time-invariant (LTI) representation:

$$x_m(k+1) = A_m x_m(k) + B_m u(k) + d \quad (5)$$

where:

$$A_m = \begin{bmatrix} 1 - \dfrac{R\Delta t}{L} & \omega_n\Delta t \\ -\omega_n\Delta t & -\dfrac{R\Delta t}{L} \end{bmatrix}, \quad B_m = \begin{bmatrix} \frac{\Delta t}{L} & 0 \\ 0 & \frac{\Delta t}{L} \end{bmatrix}. \quad (6)$$

The term $d = [0 \quad -\frac{\omega_n\lambda_m\Delta t}{L}]^T$ represents the constant disturbance vector. Here, $k \in \mathbb{N}$ denotes the discrete-time index, while $x_m(k) = [i_d(k) \quad i_q(k)]^T$ and $u(k) = [u_d(k) \quad u_q(k)]^T$ represent the state and manipulated input vectors, respectively.

Given the high sampling rates inherent in power electronic applications, the forward Euler approximation provides a reliable discretization with negligible discretization error [2], [3].

The system output vector, comprising the d-q axis stator currents, is defined as:

$$\bar{y}(k) = C_m x_m(k), \quad (7)$$

where $C_m = I_{2\times 2}$.

Equations (5) and (7) constitute the prediction plant model used by the MPC controller to solve the constrained optimization problem at each sampling interval.

Fundamentally, the design of discrete-time MPC centers on the receding horizon optimization of the future control trajectory. Building upon the methodology proposed in [11], this study derives an MPC formulation that utilizes a set of discrete-time Laguerre functions to provide a high-fidelity, reduced-parameter approximation of the predicted future control sequence.

A. Control signal trajectory described by Laguerre functions

Following the approach proposed in [11], a set of discrete orthonormal functions is used to represent the trajectory of the future control signal difference over a moving horizon window. Specifically, Laguerre functions are selected as the orthonormal basis for this purpose. Accordingly, for a set of Laguerre functions, $\ell_1(k), \ell_2(k), \ldots, \ell_N(k)$ [11]:

$$\Delta u(k_i + k) \approx \sum_{m=1}^{N} \gamma_m(k_i)\ell_m(k) \tag{8}$$

where $\Delta u(k_i + k) = u(k_i + k) - u(k_i + k - 1)$, with k_i the initial time of the moving horizon window and k the future sampling instant. Here, N denotes the number of expansion terms and γ_m, $m = 1, 2, \ldots, N$, are the corresponding coefficients depending on k_i. As N increases, the expansion converges to the sequence $\Delta u(k_i)$, $\Delta u(k_i + 1)$, $\Delta u(k_i + 2)$, …, $\Delta u(k_i + N_c)$, where N_c is the control horizon in the conventional design [11].

References [11], [14] demonstrate that the discrete Laguerre functions satisfy the following difference equation:

$$\mathcal{L}(k+1) = \Gamma\mathcal{L}(k), \tag{9}$$

where

$$\mathcal{L}(k) = \begin{bmatrix}\ell_1(k) & \ell_2(k) & \cdots & \ell_N(k)\end{bmatrix}^T, \tag{10}$$

and

$$\Gamma = \begin{bmatrix} \alpha & 0 & 0 & \cdots & 0 \\ b & \alpha & 0 & \cdots & 0 \\ -\alpha b & b & \alpha & \cdots & 0 \\ \alpha^2 b & -\alpha b & b & \ddots & \vdots \\ \vdots & \vdots & \ddots & \ddots & 0 \\ (-1)^{N-2}\alpha^{N-2}b & (-1)^{N-3}\alpha^{N-3}b & \cdots & b & \alpha \end{bmatrix}. \tag{11}$$

where $b = 1 - \alpha^2$ with $0 \leq \alpha < 1$ the scaling factor. The scaling factor of the Laguerre polynomials modulates the decay rate of the control increments, effectively parameterizing the control horizon and shaping the closed-loop transient dynamics.

The initial condition is:

$$\mathcal{L}(0)^T = \sqrt{1-\alpha^2}\begin{bmatrix}1 & -\alpha & \alpha^2 & -\alpha^3 & \cdots & (-1)^{N-1}\alpha^{N-1}\end{bmatrix}. \tag{12}$$

B. State-space model with embedded integrator

As proposed in [11], to facilitate the design of a controller with an embedded integrator, the original model of Eqs. (5) and (7) is augmented by adopting the control increment $\Delta u(k) = u(k) - (k-1)$ as the new input. According to the methodology in [11], the augmented system is constructed as follows. Let

$$\Delta x_m(k) = x_m(k) - x_m(k-1). \tag{13}$$

By defining the augmented state vector as:

$$x(k) = \begin{bmatrix}\Delta x_m(k) & \bar{y}(k)\end{bmatrix}^T, \tag{14}$$

the augmented state-space representation is formulated as follows:

$$\begin{aligned} \underbrace{\begin{bmatrix}\Delta x_m(k+1) \\ \bar{y}(k+1)\end{bmatrix}}_{x(k+1)} &= \underbrace{\begin{bmatrix} A_m & O_2 \\ C_m A_m & I_2\end{bmatrix}}_{A}\underbrace{\begin{bmatrix}\Delta x_m(k) \\ \bar{y}(k)\end{bmatrix}}_{x(k)} \\ &+ \underbrace{\begin{bmatrix} B_m \\ C_m B_m\end{bmatrix}}_{B}\Delta u(k), \end{aligned} \tag{15}$$

$$y(k) = \underbrace{\begin{bmatrix}O_2 & I_2\end{bmatrix}}_{C}\begin{bmatrix}\Delta x_m(k) \\ \bar{y}(k)\end{bmatrix}.$$

where O_2 and I_2 are zero and unit matrices, respectively, with dimension 2×2. The resulting triplet (A, B, C) constitutes the augmented model, which serves as the basis for the subsequent predictive control design.

The electrical model of a PMSM is characterized as a multi-input multi-output (MIMO) system with two control inputs and two outputs. Consequently in (15), the control increment vector is defined as $\Delta u(k) = [\Delta u_1(k) \quad \Delta u_2(k)]^T$, and the input matrix is partitioned by columns such that $B = [B_1 \quad B_2]$, where B_i denotes the i-th column. From (8) written in a vector form, each control channel $\Delta u_i(k)$ is expanded using a Laguerre network of order N_i and scaling factor α_i according to:

$$\Delta u_i(k) = \mathcal{L}_i(k)^T\zeta_i \tag{16}$$

where $\mathcal{L}_i(k)^T = [\ell_1^i(k) \quad \ell_2^i(k) \quad \ldots \quad \ell_{N_i}^i(k)]$ is the basis vector and $\zeta_i^T = [\gamma_1^i \quad \gamma_2^i \quad \ldots \quad \gamma_{N_i}^i]$ is the coefficient vector corresponding to the initial time k_i of the moving horizon window. Considering the augmented state-space model (15) and the partition of the input matrix B, the m-step ahead state prediction is derived as [15]:

$$\begin{aligned} x(k_i + m|k_i) = A^m x(k_i) + \sum_{j=0}^{m-1} A^{m-j-1} \\ \times [B_1\mathcal{L}_1(j)^T \quad B_2\mathcal{L}_2(j)^T]\zeta \end{aligned} \tag{17}$$

where $\zeta = [\zeta_1^T \quad \zeta_2^T]^T$ represents the global vector of decision variables to be optimized. The corresponding predicted plant output is then formulated as [11]:

$$y(k_i + m|k_i) = CA^m x(k_i) + \psi(m)^T\zeta \tag{18}$$

where $\psi(m)^T = \sum_{j=0}^{m-1} CA^{m-j-1}[B_1\mathcal{L}_1(j)^T \quad B_2\mathcal{L}_2(j)^T]$ is the convolution sum relating the Laguerre coefficients to the output trajectory.

Under this formulation, the predicted state and output variables are parameterized by the Laguerre coefficient vector ζ. Consequently, ζ serves as the decision variable to be optimized during the design process.

C. Unconstrained optimal control formulation

Following the methodology in [11], let $r(k_i+m) = [r_1(k_i+m) \quad r_2(k_i+m)]^T$ denote the vector of future reference trajectories for the plant outputs (see Eq. (15)) over the prediction horizon $0 \le m \le N_p$. The objective of the MPC is to determine the optimal control sequence that minimizes the following quadratic cost functional [11]:

$$J = \sum_{m=1}^{N_p}[r(k_i+m) - y(k_i+m|k_i)]^T Q[r(k_i+m) - y(k_i+m|k_i)] + \zeta^T R\zeta \tag{19}$$

where Q and R denote symmetric positive-definite matrices. For the unconstrained case, the optimal parameter vector is derived by substituting (18) into (19) and solving for the stationary point of the cost functional:

$$\hat{\zeta} = \left(\sum_{m=1}^{N_p}\psi(m)Q\psi(m)^T + R\right)^{-1} \times \left(\sum_{m=1}^{N_p}\psi(m)Q(r(k_i+m) - CA^m x(k_i))\right) \tag{20}$$

Once the optimal parameter vector $\hat{\zeta}$ is determined, the control law is implemented according to the receding horizon principle. At each sampling instant k_i, only the first element of the optimized control trajectory is applied:

$$\Delta u(k_i) = \begin{bmatrix} \mathcal{L}_1(0)^T & 0_2^T \\ 0_1^T & \mathcal{L}_2(0)^T \end{bmatrix} \hat{\zeta} \tag{21}$$

where 0_1^T and 0_2^T denote zero block of appropriate dimensions, corresponding to the Laguerre basis vectors $\mathcal{L}_1(0)^T$ and $\mathcal{L}_2(0)^T$, respectively.

D. Laguerre-Based MPC with Explicit Constraint Handling

A primary advantage of Model Predictive Control (MPC) is its inherent capability to explicitly incorporate hard constraints within the control design. By parameterizing the control trajectory via Laguerre functions, the designer gains the flexibility to strategically select the temporal locations of future constraints. This selective enforcement can significantly reduce the total number of inequality constraints over the prediction horizon, thereby mitigating the online computational burden for large-scale systems [11]. Furthermore, the intrinsic exponential decay characteristic of Laguerre basis functions [11] ensures that control increments Δu asymptotically vanish beyond the transient phase. Consequently, imposing constraints primarily during the transient period is often sufficient to guarantee feasible operation, further streamlining the optimization problem [11].

1) Constraints on control increments [11]: The physical limitations on the rate of change of the control signals are expressed as $\Delta u^{\min} \le \Delta u(k_i+m) \le \Delta u^{\max}$. By substituting the Laguerre-based parameterization, these limits are mapped as:

$$\Delta u^{\min} \le \begin{bmatrix} \mathcal{L}_1(m)^T & 0_2^T \\ 0_1^T & \mathcal{L}_2(m)^T \end{bmatrix} \zeta \le \Delta u^{\max} \tag{22}$$

where m belongs to the set of sampling instants within the prediction horizon where constraint satisfaction is explicitly required.

2) Constraints on control magnitudes [11]: Let $u^{\min}$ and $u^{\max}$ denote the physical saturation limits of the control signals. Noting that the increment of the control signal is $u(k) = \sum_{i=0}^{k-1}\Delta u(i)$ [11], the constraints for any future time instant $k \in \{1, 2, \dots\}$ are formulated as:

$$u^{min} \le \begin{bmatrix} \sum_{i=0}^{k-1}\mathcal{L}_1(i)^T & 0_2^T \\ 0_1^T & \sum_{i=0}^{k-1}\mathcal{L}_2(i)^T \end{bmatrix} \zeta + u(k_i-1) \le u^{max}, \tag{23}$$

where $u(k_i-1)$ represents the control signal state from the previous sampling interval.

The stator voltage vector, $u = [u_d, u_q]^T$, is subject to the physical limitations of the power converter:

$$u \in \mathcal{U} = \{u \in \mathbb{R}^2 : \|u\|_2 \le U_{max}\} \tag{24}$$

where the maximum voltage $U_{\max}$ is determined by the DC-link voltage U_{dc} and the modulation strategy. For space vector modulation (SVM), this limit is established as $U_{\max} = U_{dc}/\sqrt{3}$ [2]. To preserve the linearity of the constraints and ensure compatibility with standard QP solvers, this circular constraint is approximated by a rectangular bounding box:

$$|u_q| \le \delta\frac{U_{dc}}{\sqrt{3}}, \quad |u_d| \le \sqrt{1-\delta^2}\frac{U_{dc}}{\sqrt{3}} \tag{25}$$

where $\delta \in [0, 1]$ is a scaling parameter [16]. Furthermore, constraints on the control increments Δu_d and Δu_q are enforced as a fraction of the limits in (25). This approach accounts for the finite slew rate of the power stage and prevents excessive control effort during fast transients

Given that the objective functional (19) is quadratic and the associated constraints are formulated as linear inequalities (25), the determination of the optimal predictive control law is reduced to a standard Quadratic Programming (QP) problem [17]. In this work, Hildreth's quadratic programming algorithm [17] is adopted due to its suitability for real-time embedded applications.

V. Simulation Results

To assess the validity of the proposed methodology, the highly accurate Whirlpool simulation software for household appliances was employed. Numerical analyses were performed on a model of a PMSM drain pump installed in a Whirlpool dishwasher. The nominal parameters of the PMSM are reported in Table I. The simulations were also designed to compare the performance of the proposed control strategy with that of a PI controller, which is currently implemented in several Whirlpool production units, while following the speed profile depicted in Figure 2. The selected parameters for the proposed controller are summarized in Table II. No re-tuning was applied to the PI controller, as it is already deployed in Whirlpool's production systems; thus, its parameters are assumed to be adequately and previously calibrated. Figures 3 and 4 illustrate the motor mechanical speed and electrical torque, respectively, over the simulation time interval from 5 s to 10 s. This interval corresponds to a sudden variation in load torque, caused by the complete drainage of water, simulating the condition in which the pump operates without water and the motor impeller rotates freely. During this period, the sensitivity of the PI speed control to torque drops becomes evident, resulting in a pronounced overshoot in the velocity signal. In contrast, the proposed control strategy exhibits a smaller deviation from the reference and a faster recovery following the peak. Overall, the proposed controller demonstrates superior responsiveness and accuracy compared to the conventional Proportional-Integral controller. To quantitatively evaluate the effectiveness of the control action, two performance indices were considered: the integral of absolute error (IAE) and the mean squared error (MSE). It should be noted that these indices were calculated only over the interval surrounding the torque drop, where the controllers' sensitivity is most pronounced. As reported in Table IV, the values of both indices for the proposed control are lower than those for the PI controller, highlighting the improved performance achieved by the proposed approach.

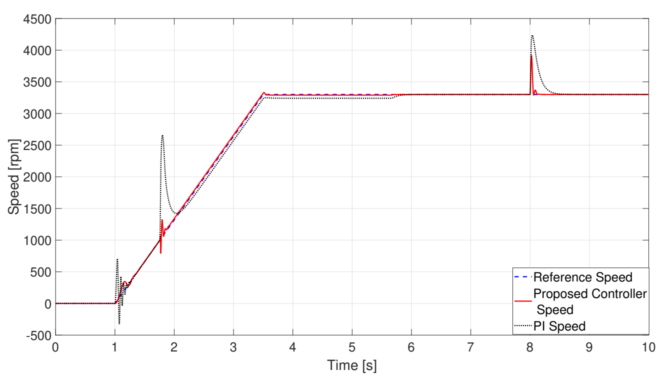

Fig. 2: Mechanical speed: Reference (blue dashed line), PI control (black dotted line), Proposed Controller (red continuous line).

VI. Robustness Tests

Robustness tests were performed to evaluate the control system's ability to maintain high performance in the presence of uncertainties, including variations in system parameters and external disturbances. In practical applications, motor parameters such as resistance, inductance, and load torque

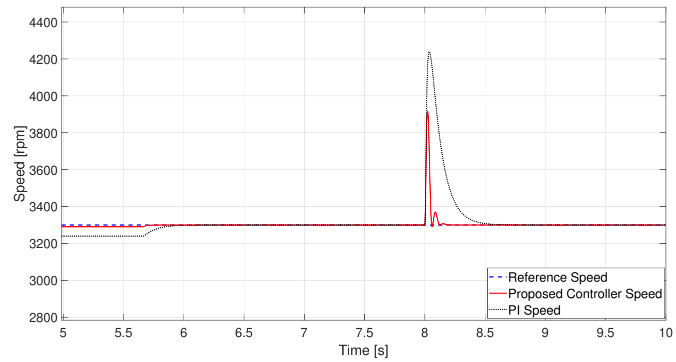

Fig. 3: Mechanical speed: load torque variation.

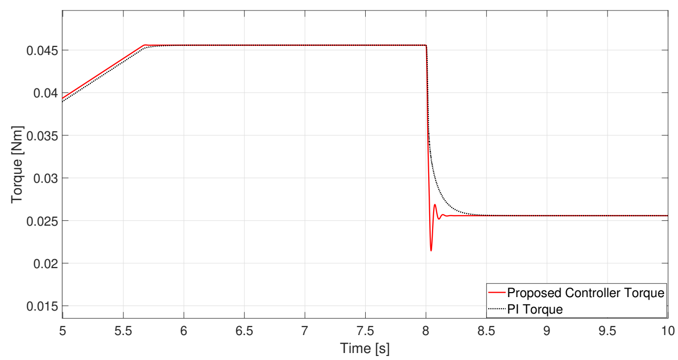

Fig. 4: Electrical torque: load torque variation.

may fluctuate due to temperature changes, mechanical wear, or external factors. These tests aimed to assess how effectively the proposed control strategy can handle such deviations while ensuring stable and precise regulation of motor speed and current. To this end, deliberate variations were applied to the motor's electromechanical parameters. Each parameter was tested at its extreme values using a Design of Experiments (DOE) methodology, which allows structured evaluation of input variations on system behavior. Specifically, each of the five parameters was individually set to its minimum or maximum, yielding 32 distinct experimental configurations. By applying boundary conditions simultaneously across all parameters, the controller's robustness was examined under demanding yet realistic scenarios. Table III summarizes the parameter values used. Simulations were carried out in a custom Simulink® environment developed by Whirlpool, with an automated MATLAB script executing all experiments. Initial runs under nominal conditions established baseline IAE (Integral Absolute Error) and MSE (Mean Squared Error) values, which were then compared with results from the varied parameter scenarios to assess performance under non-ideal conditions. Table IV reports the average metrics across the 32 tests for both the proposed controller and a conventional PI controller, enabling a detailed comparison. Performance indices were calculated over the interval from the 5th to the 10th second, which captures the sudden torque drop discussed in Section V, providing a meaningful evaluation of

TABLE I: PMSM parameters

Coil dependent parameters		
Phase-phase resistance	ohm	45.5
Phase-phase inductance	mH	120
Flux linkage	Vpk/rad/s	0.0857
Torque constant	Nm/A	0.12855
Pole pairs	–	1
Dynamic parameters		
Max. current	A peak	0.6
Max. torque	Nm	0.07
Max. speed	rpm	4000
Mechanical parameters		
Rotor inertia	$\mathrm{Kgm}^2 \cdot 10^{-6}$	2.13
Friction Coefficient	Nm/ rad/s $\cdot 10^{-5}$	7.40

TABLE II: Control scheme parameters

MPC Currents Regulator Parameters	
$\alpha = [0.7\ 0.7]$	$N_p = 40$
$R = \begin{bmatrix} 0.6 & 0 \\ 0 & 0.6 \end{bmatrix}$	$\delta = 0.32$
$N = [1\ 1]$	$\Delta u_d^{min} = -0.1$ $\Delta u_d^{max} = 0.1$
$N_c = 5$	$\Delta u_q^{min} = -0.1$ $\Delta u_q^{max} = 0.1$

the controller's robustness to abrupt load changes. The results demonstrate that the proposed controller exhibits superior robustness compared to the PI controller. Lower IAE and MSE values indicate improved tracking accuracy and reduced response variability, even under adverse operating conditions (Table IV).

TABLE III: Robustness Tests: PMSM Parameter Variations Across Temperature Ranges

Parameter	**Nominal Value**	**Min** (10°C)	**Max** (100°C)	**Unit**
Stator Resistance (R_s)	45.5	40.27	61.60	Ω
Stator Inductance (L_s)	120	111.6	128.4	mH
Flux Linkage (Φ_m)	0.0857	0.0673	0.0939	V·s/rad
Inertia Moment (J)	2.13×10^{-6}	2.02×10^{-6}	2.24×10^{-6}	kg·m^2
Friction Coefficient (B)	7.40×10^{-5}	7.03×10^{-5}	7.77×10^{-5}	N·m·s/rad

TABLE IV: Robustness Tests: Comparison of Performance Indices

Control Strategy	**IAE (Nominal)**	**MSE (Nominal)**	**IAE (Robustness)**	**MSE (Robustness)**
Standard PI Controller	18.3906	178.5726	20.1645	205.9839
Proposed Controller	3.0242	23.0168	3.4028	27.7377

VII. CONCLUSIONS

A Laguerre-based MPC algorithm was developed and validated for PMSM current regulation. The use of Laguerre basis functions allowed for an efficient description of the future control sequence, structurally reducing the number of optimization variables compared to standard CCS-MPC formulations, which is an inherent advantage for deployment on resource-constrained microcontrollers. Numerical results obtained through the high-accuracy Whirlpool simulation environment confirm that the proposed predictive controller outperforms traditional PI-based systems, offering enhanced tracking precision.

REFERENCES

[1] Z. Cao, J. Mao, C. Zhang, W. Zhao, and J. Yang, "Robust adaptive control barrier function-based model predictive speed control for pmsm drives with current safety guarantees," *IEEE Transactions on Industrial Electronics*, pp. 1–12, 2026.

[2] M. Preindl, S. Bolognani, and C. Danielson, "Model predictive torque control with pwm using fast gradient method," in *2013 Twenty-Eighth Annual IEEE Applied Power Electronics Conference and Exposition (APEC)*, 2013, pp. 2590–2597.

[3] G. Cimini, D. Bernardini, S. Levijoki, and A. Bemporad, "Embedded model predictive control with certified real-time optimization for synchronous motors," *IEEE Transactions on Control Systems Technology*, vol. 29, no. 2, pp. 893–900, 2021.

[4] Z. Mynar, L. Vesely, and P. Vaclavek, "Pmsm model predictive control with field-weakening implementation," *IEEE Transactions on Industrial Electronics*, vol. 63, no. 8, pp. 5156–5166, 2016.

[5] F. Mwasilu, E.-K. Kim, M. S. Rafaq, and J.-W. Jung, "Finite-set model predictive control scheme with an optimal switching voltage vector technique for high-performance ipmsm drive applications," *IEEE Transactions on Industrial Informatics*, vol. 14, no. 9, pp. 3840–3848, 2018.

[6] P. Karamanakos, T. Geyer, and R. P. Aguilera, "Long-horizon direct model predictive control: Modified sphere decoding for transient operation," *IEEE Transactions on Industry Applications*, vol. 54, no. 6, pp. 6060–6070, 2018.

[7] M. R. Arahal, C. Martín, F. Barrero, and M. J. Durán, "Assessing variable sampling time controllers for five-phase induction motor drives," *IEEE Transactions on Industrial Electronics*, vol. 67, no. 4, pp. 2523–2531, 2020.

[8] M. Preindl and S. Bolognani, "Model predictive direct speed control with finite control set of pmsm drive systems," *IEEE Transactions on Power Electronics*, vol. 28, no. 2, pp. 1007–1015, 2013.

[9] S. Rubino, R. Bojoi, S. A. Odhano, and P. Zanchetta, "Model predictive direct flux vector control of multi-three-phase induction motor drives," *IEEE Transactions on Industry Applications*, vol. 54, no. 5, pp. 4394–4404, 2018.

[10] M. Preindl and S. Bolognani, "Comparison of direct and pwm model predictive control for power electronic and drive systems," in *2013 Twenty-Eighth Annual IEEE Applied Power Electronics Conference and Exposition (APEC)*, 2013, pp. 2526–2533.

[11] L. Wang, "Discrete model predictive controller design using laguerre functions," *Journal of Process Control*, vol. 14, no. 2, pp. 131–142, 2004.

[12] P. Vas, *Vector control of AC machines*. London, U.K.: Oxford Univ. Press, 1990.

[13] E. Brasili, L. Fagnano, G. Ippoliti, and G. Orlando, "Discrete-time sliding mode control of pmsms for a household appliance," in *IECON 2025 – 51st Annual Conference of the IEEE Industrial Electronics Society*, 2025, pp. 1–6.

[14] B. Wahlberg, "System identification using laguerre models," *IEEE Transactions on Automatic Control*, vol. 36, no. 5, pp. 551–562, 1991.

[15] L. Wang, "Discrete time model predictive control design using laguerre functions," in *Proceedings of the 2001 American Control Conference. (Cat. No.01CH37148)*, vol. 3, 2001, pp. 2430–2435 vol.3.

[16] S. Bolognani, S. Bolognani, L. Peretti, and M. Zigliotto, "Design and implementation of model predictive control for electrical motor drives," *IEEE Transactions on Industrial Electronics*, vol. 56, no. 6, pp. 1925–1936, 2009.

[17] D. G. Luenberger, *Linear and Nonlinear Programming*, 2nd ed. New York, NY: Springer, 2003.